EDGE ARTICLE

Exploring a new short-wavelength nonlinear optical fluoride material featuring unprecedented polar *cis*-[Zr$_6$F$_{34}$]$^{10-}$ clusters†

Mei Yan, Ru-Ling Tang, [iD] * Wen-Dong Yao, Wenlong Liu [iD] and Sheng-Ping Guo [iD] *

Traditional fluorides are rarely reported as candidates for nonlinear optical (NLO) materials featuring a deep-ultraviolet cutoff edge. Theoretical investigations suggest that the ZrF$_8$ dodecahedron shows large polarizability anisotropy and benefits for large birefringence. Herein, a new fluorine-rich fluoride, K$_3$Ba$_2$Zr$_6$F$_{31}$, was synthesized by coupling the ZrF$_8$ group, featuring acentric *cis*-[Zr$_6$F$_{34}$]$^{10-}$ clusters with a 6$_3$-screw axis. Significantly, K$_3$Ba$_2$Zr$_6$F$_{31}$ exhibits a short UV cutoff edge (below 200 nm) and moderate second-harmonic generation (SHG) response (0.5 × KH$_2$PO$_4$). It also possesses a relatively large birefringence (0.08@1064 nm), together with a broad transparency window (2.5–21.1 μm). First-principles calculations suggest that the *cis*-[Zr$_6$F$_{34}$]$^{10-}$ cluster built by ZrF$_8$ dodecahedra are the dominant contributors to the large band gap (7.89 eV, cal.) and SHG response simultaneously. Such systematic work highlights that Zr-based fluorides afford a new paradigm for the development of efficient NLO materials with a short UV cutoff edge.

Introduction

Deep-ultraviolet (DUV) nonlinear optical (NLO) materials can produce coherent light below 200 nm through a second harmonic generation (SHG) process, which is useful for diverse applications in high-tech equipment and represents a leading edge in materials and civil science.[1–6] Traditionally, research on such materials has been mainly limited to π-conjugated systems, expanding from borate, carbonates like AEB$_8$O$_{15}$H$_4$ (AE = Sr, Ca),[7] β-Rb$_2$Al$_2$B$_2$O$_7$,[8] LiZn(OH)CO$_3$,[9] and K$_5$Mg$_2$La$_3$(-BO$_3$)$_6$ (ref. 10) to borate fluorides, fluorooxoborates, fluoride carbonates as RbAlB$_3$O$_6$F,[11] Cs$_{0.5}$Rb$_{0.5}$AlB$_3$O$_6$F,[11] CsB$_4$O$_6$F,[12] M$_2$B$_{10}$O$_{14}$F$_6$ (M = Ca, Sr),[13] BaBe$_2$BO$_3$F$_3$,[14] KMgCO$_3$F.[15] The latest, non-π-conjugated systems have provided a source for DUV transparent materials, and can be divided into phosphates, sulfates, silicates, and their derivatives. The discovery of LiRb$_2$PO$_4$,[16] CsNaMgP$_2$O$_7$,[17] Ba$_3$P$_3$O$_{10}$X (X = Cl, Br),[18] Li$_2$BaSiO$_4$,[6] Cs$_2$B$_4$SiO$_9$,[19] Li$_3$AlSiO$_5$,[20] and K$_2$Zn$_3$(SO$_4$)(HSO$_4$)$_2$F$_4$,[21] have attracted more scientists to consider these systems as promising candidates for DUV NLO materials and to discover more compounds.

The prerequisite of eminent NLO crystals is the ability to crystallize into noncentrosymmetric structures.[22–26] Polar materials, one branch of noncentrosymmetric (NCS)

symmetries, have been increasingly recognized as an indispensable part, along with various polar functional building blocks (FBBs). Wu's group proposed a polar iodate K$_2$-Zn(IO$_3$)$_3$(I$_2$O$_5$(OH))(IO$_2$(OH))(H$_2$O) composed of "tumbler-like" [Zn(IO$_3$)(I$_2$O$_5$(OH))] clusters.[27] Luo's group reported one DUV crystal Ba(SO$_3$CH$_3$)$_2$, with a new polar non-π-conjugated NLO building unit, SO$_3$CH$_3^-$.[28] Wu's group synthesized Zn(NH$_3$)CO$_3$ which displays a "three-in-one" NLO-active motif which includes a polar NH$_3$ molecule, polar displaced Zn^{2+}, and π-conjugated CO$_3^{2-}$ ions.[29] The polar tetrahedral S$_2$O$_3$ group constructed of one UV NLO crystal (NH$_4$)$_2$S$_2$O$_3$ was provided by Luo's group.[30] Additionally, to obtain a short UV cutoff edge, fluorine with large polarizability anisotropy and hyper-polarizability is frequently used in designing new NLO materials with a DUV cutoff edge.[31–35] The borate fluorides, fluorooxoborates, fluoride carbonates, fluoride sulfates, and fluoride phosphates mentioned above with oxyfluoride moieties, have been reported with excellent overall NLO properties. The success of synthesizing these crystals draws our attention to pure fluorides. To date, the reported three fluorides (BaMgF$_4$, BaZnF$_4$, and SrAlF$_5$) all feature short UV transparency (∼126, 155, and 145 nm).[36–38] Nevertheless, severe drawbacks of small birefringence hinder the realization of phase-matchable (PM) behaviors.

To break the limits of non-PM behavior and impart a sense of polarity into a material, our work utilizes polar metal fluoride polyhedra. We herein comprise ZrF$_8$ dodecahedra with large polarizability anisotropy and present a polar fluoride, K$_3$Ba$_2$Zr$_6$F$_{31}$, through assembling the alignment of acentric *cis*-[Zr$_6$F$_{34}$]$^{10-}$ clusters. Additionally, the K$^+$ and Ba^{2+} cations

School of Chemistry and Chemical Engineering, Yangzhou University, 180 Siwangting Road, Yangzhou 225002, P. R. China. E-mail: rltang@yzu.edu.cn; spguo@yzu.edu.cn

without d–d/f–f transition are incorporated, and we survey the K–Ba–Zr–F system in detail. Since the band gap and optical properties are mainly decided by the Zr and F atoms, and the F-2p nonbonding states are the dominant contributors for the top of the valence band, speculation about the higher ratio of F atoms in the material may lead to a shorter UV cutoff edge, leading to an increase in the quantity of HF and altered ratio of reagents. Fortunately, our endeavor results in a new polar fluoride, $K_3Ba_2Zr_6F_{31}$. The cis-$[Zr_6F_{34}]^{10-}$ clusters, formed by vertex- and edge-sharing ZrF_8 dodecahedra arranged in the same orientation, makes $K_3Ba_2Zr_6F_{31}$ exhibit a moderate SHG response and a DUV cutoff edge below 200 nm. It also features PM behavior, a large calculated band gap (7.89 eV), and large birefringence (0.08@1064 nm), which declares it as a potential NLO crystal and verifies the cis-$[Zr_6F_{34}]^{10-}$ cluster as a promising functional motif for constructing NLO materials.

Results and discussion

Colorless and transparent rod-like crystals of $K_3Ba_2Zr_6F_{31}$ were synthesized via a hydrothermal thermal reaction from a mixture of KF, ZrF_4, $BaCl_2 \cdot 2H_2O$, and HF solution at 200 °C (detailed description in the ESI†). The experimental powder X-ray diffraction (PXRD) pattern is characterized and shown in Fig. S1a,† matching well with the simulated one and confirming the purity of the powder sample. The result is also confirmed with EDS elemental analysis, as shown in Fig. S1b.†

With a polar structure, $K_3Ba_2Zr_6F_{31}$ adopts the hexagonal space group $P6_3mc$ (No. 186) (Table S1†). The asymmetric unit is made up of one unique K, one Ba, two Zr, and eight F atoms (Table S2†). The Zr(1) atom is eight-coordinated with F atoms to form a distorted ZrF_8 bicapped triangular prism with wide Zr–F distances ranging from 1.991(3) to 2.348(3) Å (Table S3†). The Zr(2) atom also exhibits an eight-coordinated mode, being bonded to F atoms with bond lengths of 2.008(3)–2.169(3) Å and forming a ZrF_8 bicapped triangular prism. Three $Zr(1)F_8$ units share edges to form the $[Zr(1)_3F_{19}]^{7-}$ cluster and three $Zr(2)F_8$ units share vertexes to form the $[Zr(2)_3F_{21}]^{9-}$ cluster (Fig. S2a and b†). The $[Zr(1)_3F_{19}]^{7-}$ and $[Zr(2)_3F_{21}]^{9-}$ clusters further share vertexes and edges to form the cis-$[Zr_6F_{34}]^{10-}$ cluster (Fig. 1a and b). The polar cis-$[Zr_6F_{34}]^{10-}$ clusters then share F(5)

atoms to generate the $\{[Zr_6F_{31}]^{7-}\}_\infty$ chain along the c-axis, which arrange parallel to the ab plane with the 6_3-screw axis (Fig. 1c). The K and Ba atoms are all bonded to twelve F atoms with bond distance ranges of $d(K–F) = 2.647(5)–3.270(5)$ Å and $d(Ba–F) = 2.795(3)–2.912(3)$ Å (Fig. S3†), situating at the space between the chains and serving as the counter ion to maintain charge balance (Fig. 1d). The BVS results of K, Ba, Zr, and F atoms are 0.92, 2.11, 4.06–4.09, 0.79–1.11, respectively, consistent with the normal valence states (Table S2†).[39]

The polymeric Zr–F clusters, linkage association modes, and dimensions of Zr-based fluorides are concluded in Table S4.† It can be seen that the hexameric clusters are common in Zr-based fluorides, and small amounts are trimeric, tetrameric, or higher octal, decameric clusters. Nevertheless, the $[Zr_6F_{34}]^{10-}$ clusters are first reported here in zirconium fluorides, distinct from the $[Zr_6F_{36}]^{12-}$, and $[Zr_6F_{38}]^{14-}$ clusters in other compounds.[40,41] The $\{[Zr_6F_{31}]^{7-}\}_\infty$ chain is also observed for the first time in $K_3Ba_2Zr_6F_{31}$, unlike the common $\{[Zr_2F_{12}]^{4-}\}_\infty$ chain in $BaZrF_6$,[42] K_2ZrF_6,[43] Li_2ZrF_6.[44] As summarized in Tables S5 and S6,† $K_3Ba_2Zr_6F_{31}$ is not only the first with an asymmetric structure among the fluorides with 31 F elements in the formula, but also the first reported to be SHG-active among the fluorine-rich fluorides (F > 30), although $(XeF)_2(Ti_9F_{38})$ and $LiK_{10}Zr_6F_{35} \cdot 2H_2O$ also crystallizes in the NCS space groups.[45,46]

The thermal behavior of $K_3Ba_2Zr_6F_{31}$ was investigated using differential thermal analysis (DTA), thermogravimetric analysis (TGA), and PXRD characterization. As seen in Fig. S4a,† no distinct weight loss was apparent from the TGA curve until 650 °C, while an endothermic peak could be observed around 490 °C on the DTA curve. In order to find out the attribution of the peak at 490 °C, the powder sample was heated to 500 °C followed by PXRD (Fig. S4b†). The XRD peaks show obvious differences with the peaks in the unheated sample, and the residues correspond to BaF_2 and $K_3Zr_2F_{11}$. The XRD pattern of the sample heated to 630 °C is similar to that of the sample heated to 500 °C, which manifests the decomposition of $K_3Ba_2Zr_6F_{31}$. The weight loss covering 650–1000 °C could be assigned to the partial decomposition of the ZrF_4, and the apparent weight loss (43.7%) detected is consistent with the calculated value (cal. 40.7%). The
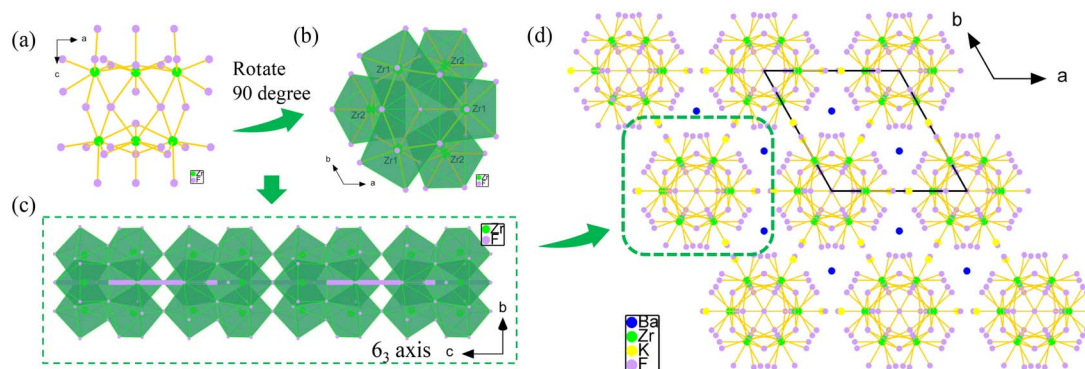

Fig. 1 (a and b) Cis-$[Zr_6F_{34}]^{10-}$ cluster at the ac and ab plane; (c) the $\{[Zr_6F_{31}]^{7-}\}_\infty$ chain along the c-axis; (d) the aligned arrangement of the $\{[Zr_6F_{31}]^{7-}\}_\infty$ anionic chains and whole structure of $K_3Ba_2Zr_6F_{31}$ viewed along the c-axis.

residues at 1000 °C are confirmed to be $Ba_4Zr_2F_{16}$ and some unknown compounds, using the PXRD results.

The UV-vis-NIR diffuse reflectance spectrum (Fig. 2a) was measured and showed that $K_3Ba_2Zr_6F_{31}$ is transparent down to 200 nm (corresponding to a band gap larger than 6.2 eV) with high reflectance exceeding 67% in the range of 200–1400 nm. The value is larger than some fluorides like KNa_2ZrF_7 (5.07 eV),[37] Na_2CeF_6 (3.89 eV),[47] and $[Cd(C_4H_6N_2)_4]_3[ZrF_7]_2$ ($C_4H_6N_2$ = 3methylpyrazole) (5.2 eV),[48] and indicates its potential application in the UV region. The IR spectrum of $K_3Ba_2Zr_6F_{31}$ exhibits one obvious peak at 474 cm^{-1}, which can be assigned to the stretching and bending vibrations of the Zr–F bonds in the ZrF_8 units (Fig. 2b).[49]

Powder SHG measurements under 1064 nm of $K_3Ba_2Zr_6F_{31}$ were performed using the Kurtz–Perry method to evaluate the NLO properties.[50] The result indicates that PM behavior can be realized since the SHG intensities gradually increase with the increase of particle size and then reach a platform (Fig. 3a). Additionally, it showcases moderate SHG efficiency of about 0.5 times that of KH_2PO_4 (KDP) in the particle size range 200–250 μm (Fig. 3b), and is comparable with reported halides with a short UV cutoff edge, like $SrAlF_5$ (0.65 × KDP).[38] In fact, the SHG intensity of $K_3Ba_2Zr_6F_{31}$ (0.5 × KDP) is relatively weak when compared with those previously reported. To further improve the SHG efficiency of halides, Cl or Br atoms may be introduced for the favorable chemical covalence and flexibility, and relatively large polarizability. Halides with mixed halogen anions tend to show enhanced overall NLO performance, as demonstrated in previous studies involving $Pb_{18}O_8Cl_{15}I_5$,[51] $Pb_7F_{12}Cl_2$,[52] and $CsZnBO_3X_2$ (X_2 = F_2, Cl_2, and FCl).[53] Additionally, the K site occupied by Rb/Cs may be helpful for larger SHG intensities for the increased polarizability of larger congener cations along with stronger interatomic interactions with adjacent F atoms, which is supported by the cases of LiA_2PO_4 (A = Rb, Cs),[54–56] and $A_3VO(O_2)_2CO_3$ (A = K, Rb, and Cs).[57–59]
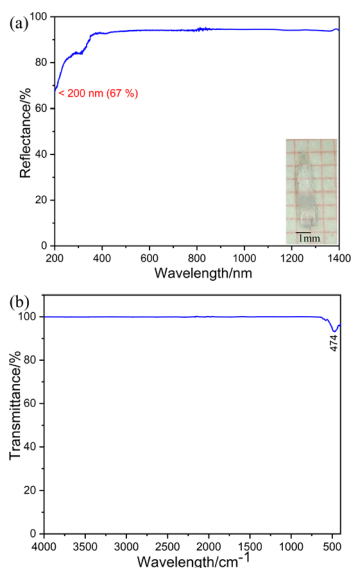
Fig. 2 (a) UV-vis-NIR diffuse reflectance and (b) IR spectra of $K_3Ba_2Zr_6F_{31}$.
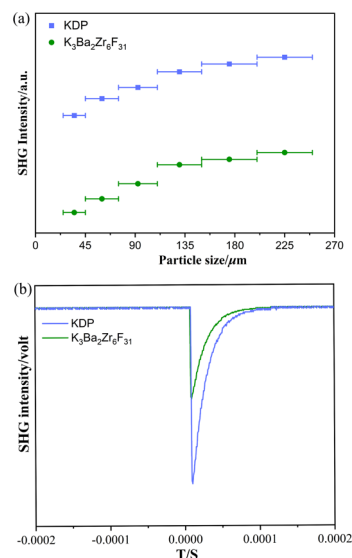
Fig. 3 (a) PM curves of $K_3Ba_2Zr_6F_{31}$ and KDP with 1064 nm laser radiation. (b) SHG intensities of $K_3Ba_2Zr_6F_{31}$ and KDP in the particle size range 200–250 μm.

In order to elucidate the origin of the SHG response, the dipole moments of ZrF_8 units have been calculated. Although the x and y components of the dipole moments in the unit cell of $K_3Ba_2Zr_6F_{31}$ did not completely offset, they only afford the values of 2.4205 and 0.0823 D in one unit cell. The z component provides much larger value of −19.8108 D that mainly determine the macroscopic polarization. The total dipole moment calculation of $K_3Ba_2Zr_6F_{31}$ affords a value of 19.9583 D for the net dipole moment in one unit cell, which corresponds with a dipole moment per unit cell of 0.034 D Å^{-3} (Table S7†). This value fits with the distorted coordination caused by the difference of the bond lengths and electronegativities, as mentioned above.

To clarify the microscopic mechanism of the properties of $K_3Ba_2Zr_6F_{31}$, theoretical calculations on the electronic structure and optical properties were performed in the CASTEP package based on density functional theory (DFT).[60,61] The calculated band structure curve shows that $K_3Ba_2Zr_6F_{31}$ has an indirect band gap of 5.79 eV with the PBE function (Fig. S5a†). The HSE06 function was also performed and the calculated value is 7.89 eV for $K_3Ba_2Zr_6F_{31}$,[62] corresponding to the very short cutoff edge of 157 nm (Fig. 4a). The underestimation of the calculated value is normal for the discontinuity of the local-density-approximation exchange–correlation function,[63–66] and the scissor of 2.1 eV was adopted when analysing the optical properties of $K_3Ba_2Zr_6F_{31}$. The total and partial density of states (TDOS and PDOS) were also calculated to investigate the interrelation of atom orbitals. The top of the valence band near the Fermi level (E_f) is mainly occupied by F-2p nonbonding states, and the bottom of the conductive band is mainly dominated by Zr-4d and F-2p orbitals (Fig. S5b†), which illustrate that the band gap of $K_3Ba_2Zr_6F_{31}$ is determined by Zr and F atoms. Considering the Kleiman symmetry restriction and the space group, $K_3Ba_2Zr_6F_{31}$ has three nonzero independent SHG coefficients, d_{15}, d_{31}, and d_{33} (Fig. 4b). The largest SHG tensor of

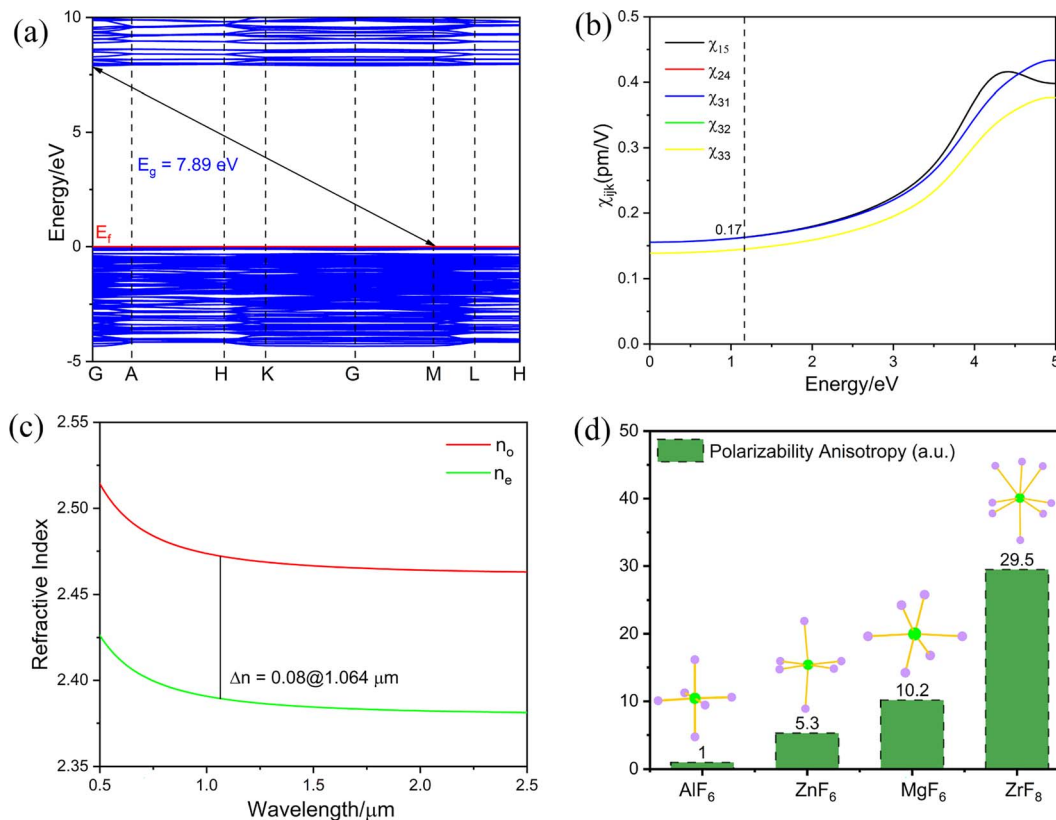Fig. 4 Calculation results for $K_3Ba_2Zr_6F_{31}$. (a) Band structure, (b) NLO coefficients, (c) refractive indexes, and (d) polarizability anisotropy of ZrF_8, MgF_6, AlF_6, and ZnF_6 species. The Fermi level is set at 0 eV.

$K_3Ba_2Zr_6F_{31}$ is calculated to be $\chi_{15} = 0.17$ pm V^{-1}, which is 0.22 times that of KDP ($d_{36} = 0.39$ pm V^{-1}). The calculated value is smaller than the experimental one ($0.5 \times$ KDP) and such underestimation has also been observed in other reports.[34,67] The birefringence (Δn) is calculated to be 0.08@1064 nm (Fig. 4c), which is larger than some d^0-TM based fluorides and oxyfluorides like $CsNaTaF_7$ (0.01@1064 nm),[68] $K_3ZrF_4(SbF_4)(SbF_5)$ (0.038@1064 nm)[49] and $K_8(ZrF_6)(Sb_2Zr_2F_{20})$ (0.039@1064 nm).[49] The birefringence (Δn) is large enough for PM ability and manifests the shortest PM wavelength (400 nm) calculated in Fig. S6.† The polarizability anisotropies of ZrF_8, MgF_6, AlF_6, and ZnF_6 species were calculated, and the value of ZrF_8 (29.5) is larger than those of the other three species (10.2, 1.0, and 5.3), illustrating the greatly enhanced birefringence and PM behaviour of $K_3Ba_2Zr_6F_{31}$ (Fig. 4d). The birefringence is large enough to realize the PM behaviour and can be attributed to the strong local polarity generated by the ordered arrangement of the $\{[Zr_6F_{31}]^{7-}\}_\infty$ chain along the c-axis.

Conclusions

In summary, a new fluorine-rich NCS fluoride with polar structure $K_3Ba_2Zr_6F_{31}$, has been studied. It features cis-$[Zr_6F_{34}]^{10-}$ clusters formed of $\{[Zr_6F_{31}]^{7-}\}_\infty$ anionic chains that formed by assembling ZrF_8 dodecahedra with large polarizability anisotropy. It is a promising NLO material with moderate

SHG response, DUV cutoff edge, and wide IR transition range. According to the theoretical calculations, it displays promising linear optical properties such as a large band gap (7.89 eV) and sufficient birefringence (0.08@1064 nm) for PM behaviour. This work opens the door to develop fluorides with polar structures composed of ZrF_8 groups with large polarizability anisotropy, beneficial for large birefringence and accelerating the development of new NLO materials with DUV cutoff edge.

Data availability

Data available in the ESI† includes experimental section, and additional tables and figures.

Author contributions

This work was conceptualised by M. Yan and R. L. Tang. Experimentation was performed by M. Yan. Software was used by W. D. Yao. W. L. Liu supervised everything. R. L. Tang and S. P. Guo contributed funding acquisition and supervision. The first draft of the manuscript was prepared by M. Yan and the final draft was edited by all the authors.

Conflicts of interest

The authors declare no competing financial interests.

Acknowledgements

Notes and references

1 M. Mutailipu, K. R. Poeppelmeier and S. L. Pan, *Chem. Rev.*, 2021, **121**, 1130–1202.

2 W. Q. Huang, S. G. Zhao and J. H. Luo, *Chem. Mater.*, 2022, **34**, 5–28.

3 Y. C. Liu, Y. G. Shen, S. G. Zhao and J. H. Luo, *Coord. Chem. Rev.*, 2020, **407**, 213152.

4 X. Liu, Y. C. Yang, M. Y. Li, L. Chen and L. M. Wu, *Chem. Soc. Rev.*, 2023, **52**, 8699.

5 F. J. Hou, D. J. Mei, M. J. Xia and Y. D. Wu, *Coord. Chem. Rev.*, 2021, **444**, 214038.

6 H. P. Wu, B. B. Zhang, H. W. Yu, Z. G. Hu, J. Y. Wang, Y. C. Wu and P. S. Halasyamani, *Angew. Chem., Int. Ed.*, 2020, **59**, 8922–8926.

7 P. F. Gong, L. Kang and Z. S. Lin, *J. Am. Chem. Soc.*, 2020, **142**, 15157–15163.

8 T. T. Tran, N. Z. Koocher, J. M. Rondinelli and P. S. Halasyamani, *Angew. Chem., Int. Ed.*, 2017, **56**, 2969–2973.

9 X. M. Liu, L. Kang, P. F. Gong and Z. S. Lin, *Angew. Chem., Int. Ed.*, 2021, **60**, 13574–13578.

10 R. Q. Liu, H. P. Wu, H. W. Yu, Z. G. Hu, J. Y. Wang and Y. C. Wu, *Chem. Mater.*, 2021, **33**, 4240–4246.

11 H. K. Liu, B. B. Zhang, L. Li and Y. Wang, *ACS Appl. Mater. Interfaces*, 2021, **13**, 30853–30860.

12 X. F. Wang, Y. Wang, B. B. Zhang, F. F. Zhang, Z. H. Yang and S. L. Pan, *Angew. Chem., Int. Ed.*, 2017, **56**, 14119–14123.

13 M. Luo, F. Liang, Y. X. Song, D. Zhao, F. Xu, N. Ye and Z. S. Lin, *J. Am. Chem. Soc.*, 2018, **140**, 3884–3887.

14 S. Guo, X. X. Jiang, L. J. Liu, M. J. Xia, Z. Fang, X. Y. Wang, Z. S. Lin and C. T. Chen, *Chem. Mater.*, 2016, **28**, 8871–8875.

15 T. T. Tran, J. Young, J. M. Rondinelli and P. S. Halasyamani, *J. Am. Chem. Soc.*, 2017, **139**, 1285–1295.

16 L. Li, Y. Wang, B. H. Lei, S. J. Han, Z. H. Yang, H. Y. Li and S. L. Pan, *J. Mater. Chem. C*, 2017, **5**, 269–274.

17 S. G. Zhao, Y. Yang, Y. G. Shen, X. D. Wang, Q. R. Ding, X. F. Li, Y. Q. Li, L. Li, Z. S. Lin and J. H. Luo, *J. Mater. Chem. C*, 2018, **6**, 3910–3916.

18 P. Yu, L. M. Wu, L. J. Zhou and L. Chen, *J. Am. Chem. Soc.*, 2014, **136**, 480–487.

19 H. P. Wu, H. W. Yu, S. L. Pan, Z. J. Huang, Z. H. Yang, X. Su and K. R. Poeppelmeier, *Angew. Chem., Int. Ed.*, 2013, **52**, 3406–3410.

20 X. L. Chen, F. F. Zhang, L. L. Liu, B. H. Lei, X. Y. Dong, Z. H. Yang, H. Y. Li and S. L. Pan, *Phys. Chem. Chem. Phys.*, 2016, **18**, 4362–4369.

21 Y. Zhou, X. Y. Zhang, Z. Y. Xiong, X. F. Long, Y. Q. Li, Y. X. Chen, X. Chen, S. G. Zhao, Z. S. Lin and J. H. Luo, *J. Phys. Chem. Lett.*, 2021, **12**, 8280–8284.

22 Y. X. Ma, P. F. Li, C. L. Hu, J. G. Mao and F. Kong, *Adv. Sci.*, 2023, **10**, 2304463.

23 Y. Huang, B. X. Li, C. L. Hu, B. P. Yang and J. G. Mao, *Inorg. Chem.*, 2023, **62**, 3343–3348.

24 S.-J. Oh, D. W. Lee and K. M. Ok, *Inorg. Chem.*, 2012, **51**, 5393–5399.

25 G. H. Zou, C. S. Lin, H. Jo, G. Nam, T.-S. You and K. M. Ok, *Angew. Chem., Int. Ed.*, 2016, **55**, 12078–12082.

26 G. H. Zou and K. M. Ok, *Chem. Sci.*, 2020, **11**, 5404–5409.

27 J. L. Chen, P. C. Yang, H. W. Yu, Z. G. Hu, J. Y. Wang, Y. C. Wu and H. P. Wu, *ACS Mater. Lett.*, 2023, **5**, 1665–1671.

28 H. T. Tian, C. S. Lin, X. Zhao, F. Xu, C. Wang, N. Ye and M. Luo, *CCS Chem.*, 2022, 1–22.

29 H. X. Tang, Q. R. Shui, R. B. Fu, Z. Q. Zhou, W. X. Bao, Z. J. Ma and X. T. Wu, *J. Mater. Chem. C*, 2021, **9**, 16477–16484.

30 S. X. Ke, H. X. Fan, C. S. Lin, N. Ye and M. Luo, *Inorg. Chem. Front.*, 2023, **10**, 2811–2817.

31 P. F. Li, C. L. Hu, F. Kong and J. G. Mao, *Angew. Chem., Int. Ed.*, 2023, **62**, e202301420.

32 B. Zhang, J. H. Wu, C. L. Hu, Y. F. Li, F. Kong and J. G. Mao, *Inorg. Chem. Front.*, 2023, **10**, 1328–1337.

33 M. Yan, R. L. Tang, W. L. Liu and S. P. Guo, *Inorg. Chem.*, 2022, **61**, 20709–20715.

34 X. Lian, W. D. Yao, W. L. Liu, R. L. Tang and S. P. Guo, *Inorg. Chem.*, 2021, **60**, 19–23.

35 E. Ko, H. Jo and K. M. Ok, *Inorg. Chem.*, 2021, **60**, 7914–7921.

36 J. G. Bergman, G. R. Crane and H. Guggenheim, *J. Appl. Phys.*, 1975, **46**, 4645–4646.

37 Y. Z. Tong, X. Y. Meng, Z. Z. Wang, C. T. Chen and M. H. Lee, *J. Appl. Phys.*, 2005, **98**, 033504.

38 E. G. Víllora, K. Shimamura, K. Muramatsu, S. Takekawa, K. Kitamura and N. Ichinose, *J. Cryst. Growth*, 2005, **280**, 145–150.

39 I. D. Brown and D. Altermatt, *Acta Crystallogr., Sect. B: Struct. Sci.*, 1985, **41**, 244–247.

40 J. H. Burns, R. D. Ellison and H. A. Levy, *Acta Crystallogr., Sect. B: Struct. Crystallogr. Cryst. Chem.*, 1968, **24**, 230–237.

41 J. P. Laval, B. Frit and J. Lucas, *J. Solid State Chem.*, 1988, **72**, 181–192.

42 J. P. Laval, R. Papiernik and B. Frit, *Acta Crystallogr. B*, 1978, **34**, 1070–1074.

43 R. Hoppe and B. Mehlhorn, *Z. Anorg. Allg. Chem.*, 1976, **425**, 200–208.

44 A. Grzechnik, V. Dmitriev and H. P. Weber, *J. Phys. Chem. Solids*, 2005, **66**, 1769–1774.

45 K. A. Gayvoronskaya, N. A. Didenko, A. B. Slobodyuk, A. V. Gerasimenko and V. Y. Kavun, *J. Fluorine Chem.*, 2011, **132**, 1159–1164.

46 K. Radan, E. Goreshnik and B. Žemva, *Angew. Chem., Int. Ed.*, 2014, **53**, 13715–13719.

47 R. L. Tang, W. Xu, X. Lian, Y. Q. Wei, Y. L. Lv, W. L. Liu and S. P. Guo, *Small*, 2023, 2308348.

48 B. Ahmed and K. M. Ok, *J. Solid State Chem.*, 2022, **309**, 122957.

49 T. K. Jiang, S. N. Yan, C. L. Hu, Y. F. Li, F. Kong and J. G. Mao, *Inorg. Chem.*, 2022, **61**, 4801–4805.

50 S. K. Kurtz and T. T. Perry, *J. Appl. Phys.*, 1968, **39**, 3798–3813.

51 X. L. Chen, Q. Jing and K. M. Ok, *Angew. Chem., Int. Ed.*, 2020, **59**, 20712.

52 Q. Wu, X. Liu, F. Liang, S. R. Xu, H. B. Pi, X. Han, Y. Liu, Z. S. Lin and Y. J. Li, *Dalton Trans.*, 2019, **48**, 13529–13535.

53 J. J. Zhou, Y. Q. Liu, H. P. Wu, H. W. Yu, Z. S. Lin, Z. G. Hu, J. Y. Wang and Y. C. Wu, *Angew. Chem., Int. Ed.*, 2020, **59**, 19006–19010.

54 X. Y. Cheng, M. H. Whangbo, G. C. Guo, M. C. Hong and S. Q. Deng, *Angew. Chem., Int. Ed.*, 2018, **57**, 3933–3937.

55 L. Li, Y. Wang, B. H. Lei, S. J. Han, Z. H. Yang, K. R. Poeppelmeier and S. L. Pan, *J. Am. Chem. Soc.*, 2016, **138**, 9101–9104.

56 L. Li, Y. Wang, B. H. Lei, S. J. Han, Z. H. Yang, H. Y. Li and S. L. Pan, *J. Mater. Chem. C*, 2017, **5**, 269–274.

57 G. H. Zou, H. Jo, S. Lim, T. You and K. M. Ok, *Angew. Chem., Int. Ed.*, 2018, **57**, 8619–8622.

58 G. H. Zou, Z. Lin, H. M. Zeng, H. Jo, S. Lim, T. You and K. M. Ok, *Chem. Sci.*, 2018, **9**, 8957–8961.

59 Y. X. Song, M. Luo, F. Liang, N. Ye and Z. S. Lin, *Chem. Commun.*, 2018, **54**, 1445–1448.

60 J. C. Stewart, D. S. Matthew, J. P. Chris, J. H. Phil, I. J. P. Matt, R. Keith and C. P. Mike, *Z. Kristallogr.–Cryst. Mater.*, 2005, **220**, 567–570.

61 M. D. Segall, P. J. D. Lindan, M. J. Probert, C. J. Pickard, P. J. Hasnip, S. J. Clark and M. C. Payne, *J. Phys.: Condens. Matter*, 2002, **14**, 2717.

62 J. Paier, M. Marsman, K. Hummer, G. Kresse, I. C. Gerber and J. G. Ángyán, *J. Chem. Phys.*, 2006, **124**, 154709.

63 B. W. Liu, X. M. Jiang, H. Y. Zeng and G. C. Guo, *J. Am. Chem. Soc.*, 2020, **142**, 10641–10645.

64 H. D. Zhou, L. Xiong, L. Chen and L. M. Wu, *Angew. Chem., Int. Ed.*, 2019, **58**, 9979–9983.

65 A. K. Iyer, S. H. Ha, M. J. Waters, T. S. Ie, S. H. Shin, J. M. Rondinelli, J. I. Jang and M. G. Kanatzidis, *Chem. Mater.*, 2023, **35**, 8706–8713.

66 Y. K. Lian, R. A. Li, X. Liu, L. M. Wu and L. Chen, *Cryst. Growth Des.*, 2020, **20**, 8084–8089.

67 W. H. Xing, C. L. Tang, N. Z. Wang, C. X. Li, E. Uykur, J. Y. Wu, Z. S. Lin, J. Y. Yao, W. L. Yin and B. Kang, *Adv. Opt. Mater.*, 2021, **9**, 2100563.

68 R. L. Tang, X. Lian, X. H. Li, L. Huai, W. L. Liu and S. P. Guo, *Chem.–Eur. J.*, 2022, **28**, e202201588.